Inductive Superconducting Quantum Interference Proximity Transistor: the L-SQUIPT

Federico Paolucci [ID],[1, *] Paolo Solinas,[2, 3] and Francesco Giazotto [ID][1, †]

[1]*NEST, Istituto Nanoscienze-CNR and Scuola Normale Superiore, I-56127 Pisa, Italy*
[2]*Dipartimento di Fisica, Università di Genova, via Dodecaneso 33, I-16146, Genova, Italy*
[3]*INFN - Sezione di Genova, via Dodecaneso 33, I-16146, Genova, Italy*

The design for an *inductive* superconducting quantum interference proximity transistor with enhanced performance, the L-SQUIPT, is presented and analyzed. The interferometer is based on a double-loop structure, where each ring comprises a superconductor-normal metal-superconductor mesoscopic Josephson weak-link and the read-out electrode is implemented in the form of a superconducting tunnel probe. Our design allows both to improve the coupling of the transistor to the external magnetic field and to increase the characteristic magnetic flux transfer functions, thereby leading to an improved ultrasensitive quantum limited magnetometer. The L-SQUIPT behavior is analyzed in both the *dissipative* and the *dissipationless* Josephson-like operation modes, in the latter case by exploiting both an inductive and a dispersive readout scheme. The improved performance makes the L-SQUIPT promising for magnetic field detection as well as for specific applications in quantum technology, where a responsive dispersive magnetometry at milliKelvin temperatures is required.

I. INTRODUCTION

The superconducting quantum interference device (SQUID) is currently one of the most used magnetometers on the market [1]. A SQUID consists of a superconducting ring interrupted by two Josephson junctions, thus its critical current strongly depends on the magnetic flux (Φ) piercing the loop [2]. To achieve sizable sensitivities, SQUIDs typically employ large pickup loops, yielding a best intrinsic flux noise on the order of $\sim 1 \; \mu\Phi_0/\sqrt{\text{Hz}}$ [1], where $\Phi_0 = 2.067 \times 10^{-15}$ Wb is the magnetic flux quantum. Differently, scanning nanoscale SQUIDs showed a flux noise as low as 50 $\text{n}\Phi_0/\sqrt{\text{Hz}}$ thanks to low inductance loops and the vicinity to the magnetic moment source [3].

Last decade witnessed the advent of another sensitive magnetometer: the superconducting quantum interference proximity transistor (SQUIPT) [4]. It is realized in the form of a superconducting ring embodying a normal metal (SNS) [5–10] or superconducting (SS$_1$S) [11–13] nanowire Josephson junction. Thanks to the superconducting proximity effect [14, 15], a phase-dependent minigap (E_g) appears in the density of states (DoS) of the nanowire [16]. The latter is modulated by the superconducting phase difference built across the nanowire generated by the magnetic flux piercing the superconducting ring. In the SQUIPT, the read-out operation is typically performed by recording the Φ-dependent current versus voltage characteristics of a tunnel probe (normal metal or superconductor) directly coupled to the proximitized Josephson junction.

The best experimental sensitivity achieved so far in a SNS-SQUIPT reaches $500 \; \text{n}\Phi_0/\sqrt{\text{Hz}}$ at 240 mK [6], while it gets about $260 \; \text{n}\Phi_0/\sqrt{\text{Hz}}$ at 1 K for a SS$_1$S device [12]. These values are a few orders of magnitude larger than the limiting theoretical flux noise of about 1 $\text{n}\Phi_0\sqrt{\text{Hz}}$ [17], because the SQUIPT magnetometer shows different weaknesses and structural drawbacks. In particular, the SQUIPT suffers from low coupling between the external magnetic field and the superconducting loop. Indeed, a conventional device needs a small loop in order to have a negligibly small ring inductance compared to the junction Josephson inductance. Only under this assumption, the full phase bias occurs across the proximitized junction thereby allowing an efficient flux-induced modulation of the DoS of the weak-link. Furthermore, the phase biasing of the junction is efficient only for an almost-sinusoidal current-phase-relation (CPR), since in such a case the Josephson inductance of the weak-link at $\Phi_0/2$ is always finite [18, 19]. By contrast, a sizable sensitivity of the SQUIPT would be achieved by exploiting nanowire junctions in the *short* limit ($\Delta_0 \leq \hbar D/L^2$, where Δ_0 is the zero-temperature gap of the superconductor, $\hbar$ is the reduced Planck constant, while D and L are the diffusion constant and the physical length of the nanowire, respectively) [11, 20, 21], since in this regime the CPR is a non-sinusoidal function of the phase (φ) [18, 19]. Yet, in the *short* limit and for low temperatures, the Josephson inductance is effectively vanishing at $\Phi \to \Phi_0/2$ thus preventing the full phase biasing of the junction. Therefore, a conventional SQUIPT needs to be operated at higher temperatures, where the Josephson inductance is finite, but the sensitivity can be sizeably reduced. Furthermore, fully superconducting SQUIPTs in the *long*-junction limit present CPRs hysteretic with direction of the external magnetic flux [11, 22], thus hampering their application as magnetometers.

Here, we propose an inductive superconducting quantum interference proximity transistor (i.e., the L-SQUIPT) that solves the above described intrinsic limitations typical of conventional SQUIPT

magnetometers. To this end, the L-SQUIPT takes advantage of a double loop geometry to efficiently bias the second SNS Josephson junction assumed to be in the *short* limit. Furthermore, by employing a superconducting tunnel probe, the L-SQUIPT read-out operation can be realized either through a dissipative (quasiparticle tunneling) or via dissipationless (Josephson supercurrent) measurements depending on the requirements of the specific application. The L-SQUIPT is predicted to show a best quantum limited noise as low as a few $n\Phi_0/\sqrt{Hz}$, thus improving the sensitivity achievable with conventional SQUIPT and SQUID magnetometers. This makes the L-SQUIPT potentially relevant for magnetic field detection as well as for other applications in the field of quantum technologies [23].

The article is organized as follows: Sec. II presents the structure of the L-SQUIPT and the basic equations describing the SNS Josephson junctions embedded in the superconducting rings; Sec. III shows the phase-biasing of the output SNS Josephson junction by the external magnetic flux; Sec. IV describes the dissipative read-out of the L-SQUIPT in both voltage and current bias operation; Sec. V presents the dissipationless read-out realized by means of inductive and dispersive measurement schemes; and Sec. VI resumes the concluding remarks.

II. STRUCTURE

The L-SQUIPT is composed of two superconducting loops each of them interrupted by a normal metal weak-link forming a SNS Josephson junction, as shown in Fig. 1-a. The first loop (of inductance L_1) converts the external magnetic flux (Φ_1) into a superconducting phase drop (φ_1) across the Josephson junction (J_1, orange), i.e., it operates a flux-to-phase conversion ($\Phi_1 \rightarrow \varphi_1$). In order to have an efficient coupling to the external magnetic field, the first superconducting loop needs, in principle, to be sufficiently large. To optimize the $\Phi_1 \rightarrow \varphi_1$ conversion, the CPR of I_{J1} is supposed to be sinusoidal (*long*-junction limit), that is [18]

$$I_{J1}(T) = I_{C1}(T)\sin(\varphi_1),\qquad(1)$$

where $I_{C1}(T)$ is the temperature-dependent critical current of the J_1 junction and T is the temperature. A simplified equation for the critical current of J_1 can be found in the high temperature regime, that is for $k_B T > 5E_{Th}$ where k_B is the Boltzmann constant and $E_{th} = \hbar D/L^2$ is the Thouless energy (with $\hbar$ the reduced Planck constant, D the diffusion coefficient of N and L the physical length of the junction). In this limit it reads

$$I_{C1}(T) = \frac{64\pi k_B T}{e R_1}\sum_{n=0}^{\infty}\frac{\sqrt{\frac{2\omega_n}{E_{Th}}}\Delta^2(T)\exp\left[-\sqrt{\frac{2\omega_n}{E_{Th}}}\right]}{[\omega_n + \Omega_n + \sqrt{2(\Omega_n^2 + \omega_n\Omega_n)}]^2},\qquad(2)$$
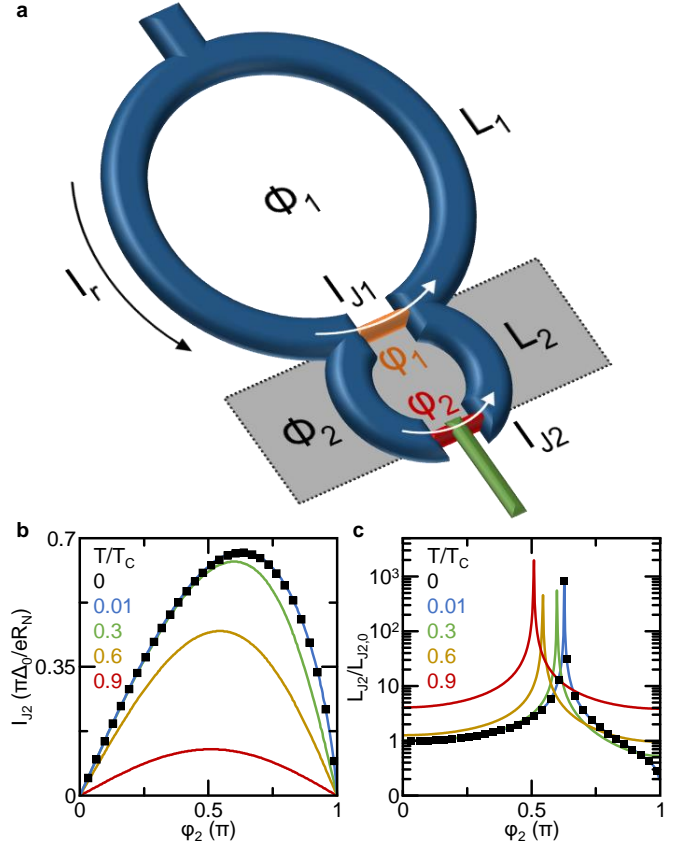

Figure 1. **(a)** Scheme of the L-SQUIPT. The device is composed by two superconducting loops of inductance L_1 and L_2 interrupted by the two SNS Josephson junctions (J_1 and J_2) of critical current I_{J1} and I_{J2}, respectively. The second ring is supposed to be screened against the external magnetic field ($\Phi_2 = 0$). Therefore, the phase drop across the two junctions is equal ($\varphi_1 = \varphi_2$). **(b)** Kulik-Omel'yanchuk current-to-phase relation (KO-CPR) of J_2 calculated in the short junction limit for different values of temperature. **(c)** Normalized Josephson kinetic inductance ($L_{J2}/L_{J2,0}$) calculated from the KO-CPR. $L_{J2,0}$ is the zero-temperature and zero-phase kinetic inductance of J_2.

where e is the electron charge, R_1 is the normal-state resistance of the junction, $\Delta(T)$ is the temperature-dependent superconducting energy gap of the ring, $\omega_n(T) = (2n + 1)\pi k_B T$ is the Matsubara frequency, and $\Omega_n(T) = \sqrt{\Delta^2(T) + \omega_n^2(T)}$.

The second loop (of inductance L_2) is supposed to be fully screened from the external magnetic field ($\Phi_2 = 0$), for instance through a superconducting plate (grey rectangle in Fig. 1-a), and operates as a phase-to-phase ($\varphi_1 \rightarrow \varphi_2$) transformer. L_2 needs to be sufficiently small in order to limit the phase drop along the smaller superconducting ring and, thus, to maximize the efficiency of the $\varphi_1 \rightarrow \varphi_2$ transformation. The junction J_2 (red) is supposed to be in the *short* limit, thus obeying to the Kulik-Omel'yanchuk (KO) model [24]. Therefore, the temperature dependent CPR of a

J_2 takes the form

$$I_{J_2}(\varphi_2, T) = \frac{\pi \Delta(T)}{eR_2} \Xi(\varphi_2, T), \qquad (3)$$

where R_2 is the normal-state resistance of J_2. The phase dependence in the KO model takes the form [24]

$$\Xi(\varphi_2, T) = \cos\left(\frac{\varphi_2}{2}\right) \times$$

$$\int\limits_{\Delta(T)\cos\left(\frac{\varphi_2}{2}\right)}^{\Delta(T)} \frac{\tanh\frac{\epsilon}{k_B T}}{\sqrt{\epsilon^2 - \Delta^2(T)\cos^2\left(\frac{\varphi_2}{2}\right)}} d\epsilon. \qquad (4)$$

In the zero-temperature limit ($T = 0$), the KO CPR can be simplified in [24]

$$I_{J_2}(\varphi_2, T = 0) = \frac{\pi \Delta_0}{eR_2} \cos\left(\frac{\varphi_2}{2}\right) \text{arctanh}\left[\sin\left(\frac{\varphi_2}{2}\right)\right], \qquad (5)$$

where Δ_0 is the zero-temperature superconducting energy gap of the ring.

Figure 1-b shows the normalized CPR of J_2 [$I_{J_2}(T)/I_{C2,0}$, with $I_{C2,0} = \frac{\pi \Delta_0}{eR_2}$ the zero-temperature junction critical current] as a function of φ_2 for different values of temperature (normalized with respect to the critical temperature T_C). By rising T, the CPR evolves from a skewed to a perfect sinusoidal phase-dependence [18, 24]. This behavior entails the higher responsivity of J_2 when the L-SQUIPT is operated at low temperature. Notably, the CPR is almost the same for the $T = 0$ limit (black squares) and for $T = 0.01T_C$ (cyan line), as shown in Fig. 1-b.

The resulting temperature-dependent Josephson inductance (L_{J_2}) of J_2 can be written as

$$L_{J_2}(\varphi_2, T) = \frac{\hbar}{2e} \frac{d\varphi_2}{dI_{J_2}(\varphi_2, T)}. \qquad (6)$$

In the zero-temperature limit, the kinetic inductance can be obtained by substituting Eq. 5 in the above expression. The resulting closed form is therefore

$$L_{J_2}(\varphi_2, T = 0) = \frac{I_{C2,0}}{2e} /$$

$$\left[-\frac{1}{2}\sin\left(\frac{\varphi_2}{2}\right)\text{artanh}\left[\sin\left(\frac{\varphi_2}{2}\right)\right] + \frac{\cos^2\left(\frac{\varphi_2}{2}\right)}{2 - 2\sin^2\left(\frac{\varphi_2}{2}\right)}\right] (7)$$

Figure 1-c shows the normalized Josephson inductance $L_{J2}/L_{J2,0}$ (with $L_{J2,0}$ its zero-temperature and zero-phase value) as a function of φ_2 calculated for different temperatures. At low temperature ($T \leq 0.3T_C$) and for $\varphi_2 \to \pi$, the Josephson inductance drops of about one order of magnitude with respect to $L_{J2,0}$. Furthermore, in the limit of $\varphi_2 \to \pi$, the zero-temperature kinetic inductance (see Eq. 7) goes to zero. As a matter of fact, the vanishing of L_{J_2} would not allow to efficiently phase-bias the Josephson junction in a conventional SQUIPT, since its inductance
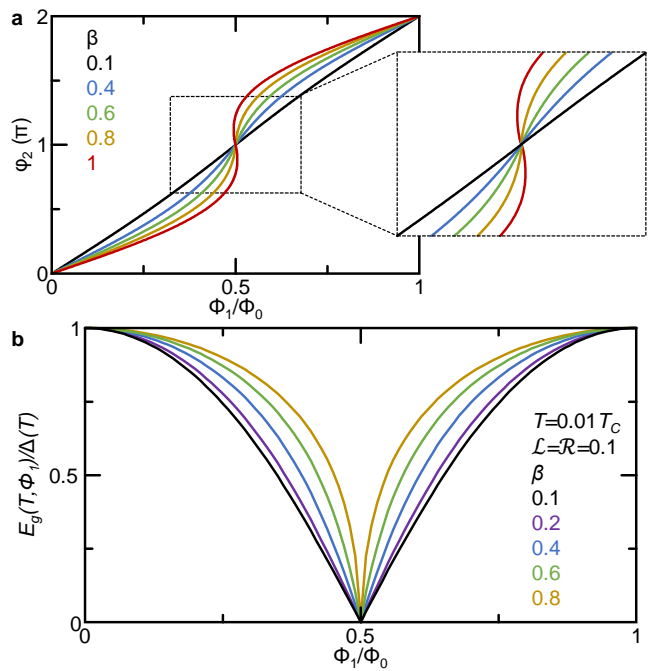

Figure 2. (a) Phase drop (φ_2) across J_2 as a function of the external flux Φ_1 calculated assuming $T = 0.01T_C$ and $\mathcal{L} = \mathcal{R} = 0.1$ for different values of β. Inset: blow up of the φ_2 versus Φ_1 characteristics calculated around $\Phi_1 = 0.5\Phi_0$. (b) Minigap induced in J_2 (E_g) as a function of Φ_1 calculated at $\mathcal{L} = \mathcal{R} = 0.1$ and $T = 0.01T_C$ for different values of β.

becomes smaller than that of the ring (L_2). As we shall show below, the L-SQUIPT allows to exploit the full phase bias of J_2 yielding largely enhanced transfer functions even at the lowest temperatures, where the magnetometer is expected to show its maximum magnetic flux sensitivity.

To perform the read-out operation, the weak-link J_2 is equipped with a superconducting readout tunnel-probe (P, green electrode in Fig. 1-a), as in conventional SQUIPTs [17]. On the one hand, this geometry allows to operate the magnetometer by conventional quasiparticle transport measurements in both voltage and current bias. On the other hand, the Φ_1-dependent Josephson coupling between J_2 and P can be employed to design different dissipationless read-out schemes for the L-SQUIPT. In particular, the variation of the Josephson output tunnel junction inductance (L_{out}) can be detected by an inductively coupled SQUID read-out or by dispersive microwave measurements.

III. PHASE-BIASING J_2

The dependence of the phase drop φ_2 across J_2 on the external magnetic flux Φ_1 can be calculated by considering three conditions typical of Josephson interferometers: (i) the quantization of the magnetic flux

piercing the first loop; (ii) the phase-locking between J_1 and J_2; (iii) the circulating supercurrent conservation in the L-SQUIPT double-loop.

Thanks to the flux quantization, the phase drop across J_1 is related to Φ_1 through

$$\varphi_1 + \frac{2\pi L_1}{\Phi_0}I_R = \frac{2\pi\Phi_1}{\Phi_0}, \tag{8}$$

where I_R is the total supercurrent circulating in the L-SQUIPT, and $\Phi_0 = 2.067 \times 10^{-15}$ Wb is the flux quantum. Equation 8 describes the $\Phi_1 \rightarrow \varphi_1$ conversion by taking into account the finite inductance L_1 of the first superconducting ring necessary to efficiently couple the L-SQUIPT to the external magnetic field. Furthermore, the phase drop φ_2 across J_2 is locked to φ_1 by the equation

$$\varphi_2 - \varphi_1 + \frac{2\pi L_2}{\Phi_0}I_{J_2} = 0, \tag{9}$$

since the magnetic flux through the second ring is assumed to be zero ($\Phi_2 = 0$). Equation 9 illustrates the $\varphi_1 \rightarrow \varphi_2$ conversion, which is strongly influenced by the finite inductance of the second ring (L_2).

Finally, to calculate the $\varphi_2(\Phi_1)$ characteristics, we need to consider the conservation of the circulating current in the L-SQUIPT. This implies that I_R is distributed between the two Josephson junctions J_1 and J_2, that is

$$I_R = I_{J_1} + I_{J_2}. \tag{10}$$

As a result, the phase drop across J_2 as a function of the external flux piercing the first loop reads

$$\varphi_2 = \frac{2\pi\Phi_1}{\Phi_0} - \beta\Big\{ \sin\left[\varphi_2 + \beta\mathcal{L}\mathcal{R}\Xi(\varphi_2)\right] + \mathcal{R}\Xi(\varphi_2)(1+\mathcal{L})\Big\}, \tag{11}$$

where $\beta = (2\pi L_1 I_{C1})/\Phi_0$ is the screening parameter accounting for the finite inductance L_1 of the first loop, $\mathcal{L} = L_2/L_1$ describes the difference between the inductance of the two loops, and $\mathcal{R} = I_{C2,0}/I_{C1,0}$ takes into account the asymmetry in the critical current of J_1 and J_2. We note that to have an efficient $\Phi_1 \rightarrow \varphi_2$ transduction, the ring inductance of the two loops need to satisfy $L_1 \gg L_2$, that is $\beta \ll 1$ is required in Eq. 11.

Figure 2-a shows the $\varphi_2(\Phi_1)$ characteristics calculated by solving Eq. 11 for different values of β at $\mathcal{L} = \mathcal{R} = 0.1$ and $T = 0.01T_C$. When the inductance of the first loop is large, the phase bias shows a strong non-linearity with Φ_1. In particular, φ_2 shows multiple solutions for $\beta \gtrsim 0.8$ in the flux range $\Phi_1 \rightarrow \Phi_0$ thereby preventing to fully phase-bias J_2. By contrast, for lower values of β, the phase drop is a continuous function of the external magnetic flux, thus J_2 is sensitive to each value of Φ_1. In the following, we will use $\beta = 0.8$ to optimize the phase-bias of J_2 and, therefore, to maximize the sensitivity of the L-SQUIPT magnetometer. We note that J_2 shows a vanishing inductance in these conditions,

since it operates in the *short*-junction limit and at low temperatures (see Fig. 1-b). Therefore, an efficient phase-bias of the junction would be impossible in a conventional SQUIPT.

The Φ_1-dependent values of φ_2 strongly influence the DoS ($\mathcal{N}_{J2}$) of the normal metal element forming the output Josephson junction. Since J_2 is assumed to be in the *short*-junction limit, its DoS takes the form [21, 25]

$$\mathcal{N}_{J2}(x,\varepsilon,\varphi_2) = \mathrm{Re}\sqrt{\frac{(\varepsilon+i\Gamma)^2}{(\varepsilon+i\Gamma)^2 - \Delta^2(T)\cos^2(\varphi_2/2)}} \times$$
$$\cosh\left(\frac{2x-L}{L}\mathrm{arccosh}\sqrt{\frac{(\varepsilon+i\Gamma)^2 - \Delta^2(T)\cos^2(\varphi_2/2)}{(\varepsilon+i\Gamma)^2 - \Delta^2(T)}}\right), \tag{12}$$

where ε is the energy relative to the chemical potential of the superconductors, Γ is the Dynes broadening parameter [26] and $x \in [0, L]$ is the spatial coordinate along the J_2 length. Equation 12 highlights that the density of states is strongly tuned by φ_2. In particular, the superconducting minigap induced in N by the proximity to S [14] takes the form

$$E_g(T,\varphi_2) = \Delta(T)\cos\left(\frac{\varphi_2}{2}\right). \tag{13}$$

We note that the value of E_g is constant along the nanowire length. For $\varphi_2 = 0$ the induced minigap is maximum [$E_g(T,0) = \Delta(T)$], while for $\varphi_2 = \pi$ the nanowire shows the normal metal DoS [$E_g(T,\pi) = 0$].

In the L-SQUIPT, the dependence of the minigap on the external magnetic flux [$E_g(T,\Phi_1)$] can be calculated by combining Eqs. 11 and 13. Figure 2-b presents the dependence of $E_g(T)$ on Φ_1 calculated at $T = 0.01T_C$ and $\mathcal{L} = \mathcal{R} = 0.1$ for different values of β. By enhancing the screening parameter, the minigap shows a stronger variation with external magnetic flux at $\Phi_1 \rightarrow 0.5\Phi_0$. On the contrary, the minigap is more sensitive at $\Phi_1 \rightarrow \Phi_0$ for low values of β, but its maximum steepness is limited. Therefore, the L-SQUIPT magnetometer is expected to show higher sensitivity for large values of β at $\Phi_1 \rightarrow 0.5\Phi_0$.

IV. DISSIPATIVE READ-OUT

Here, we discuss the magnetic flux dependent quasiparticle transport between J_2 and P. This will allow us to evaluate the sensitivity of the L-SQUIPT magnetometer both in the voltage-bias and current-bias configurations.
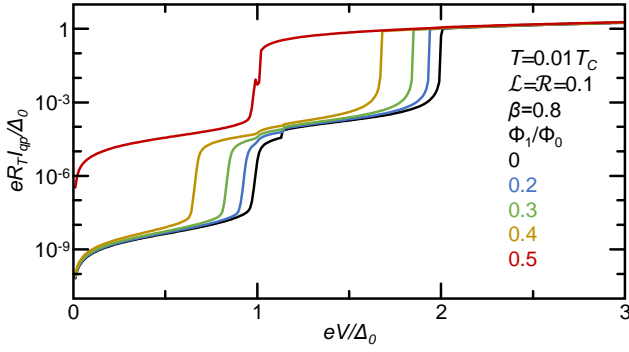
Figure 3. Quasiparticle current as a function of voltage calculated at $\beta = 0.8$ and $\mathcal{L} = \mathcal{R} = 0.1$, $T = 0.01T_C$ for several values of Φ_1. All the curves assume $\Gamma = 10^{-4}\Delta_0$.

A. Quasiparticle transport

The quasiparticle current flowing through the J_2-P tunnel junction can be written as [17]

$$I_{qp} = \frac{1}{ewR_T} \int_{\frac{L-w}{2}}^{\frac{L+w}{2}} dx \int_{-\infty}^{\infty} d\varepsilon \mathcal{N}_{J2}(x, \varepsilon, \varphi_2)\mathcal{N}_p(\varepsilon, V)\mathcal{F}(\varepsilon, V),$$

(14)

where R_T and w are the normal-state resistance and the width of the junction, respectively. Furthermore, $\mathcal{F}(\varepsilon, V) = [f_0(\varepsilon - eV) - f_0(\varepsilon)]$ is the difference between the Fermi-Dirac distribution functions (f_0) of the two electrodes. The normalized Bardeen-Cooper-Schrieffer (BCS) DoS of the superconducting tunnel probe can be written as

$$\mathcal{N}_p(\varepsilon, V) = \left| \text{Re} \left[\frac{(\varepsilon - eV + i\Gamma)}{\sqrt{(\varepsilon - eV + i\Gamma)^2 - \Delta^2(T)}} \right] \right|.$$

(15)

For simplicity, we assume the P to be made of the same superconductor of the L-SQUIPT ring.

The typical quasiparticle current (I_{qp}) versus voltage (V) characteristics of the L-SQUIPT calculated assuming $\beta = 0.8$, $\mathcal{L} = \mathcal{R} = 0.1$ and $T = 0.01T_C$ are shown in Fig. 3 for several values of the external magnetic flux. The quasiparticle current tunnels through the barrier when the voltage bias is larger than the sum of the energy gaps of J_2 and P, that is for $eV \geq \Delta(T) + E_g(T, \Phi_1)$ [27]. Indeed, the threshold voltage is maximal for $\Phi_1 = 0$ (black curve), since the minigap in N acquires the same value of the energy gap of the superconducting ring [$E_g(T, 0) = \Delta(T)$]. By rising the external magnetic flux, large quasiparticle tunneling occurs at lower values of voltage bias until reaching its minimum value $eV = \Delta(T)$ for $\Phi_1 = 0.5\Phi_0$ [red curve, since $E_g(T, 0.5\Phi_0) = 0$]. The variation of the $I_{qp}(V)$ characteristics with the magnetic flux is stronger in the interval $0.4\Phi_0 \leq \Phi_1 \leq 0.5\Phi_0$, since E_g shows a stark dependence on Φ_1 in this range (see Fig.
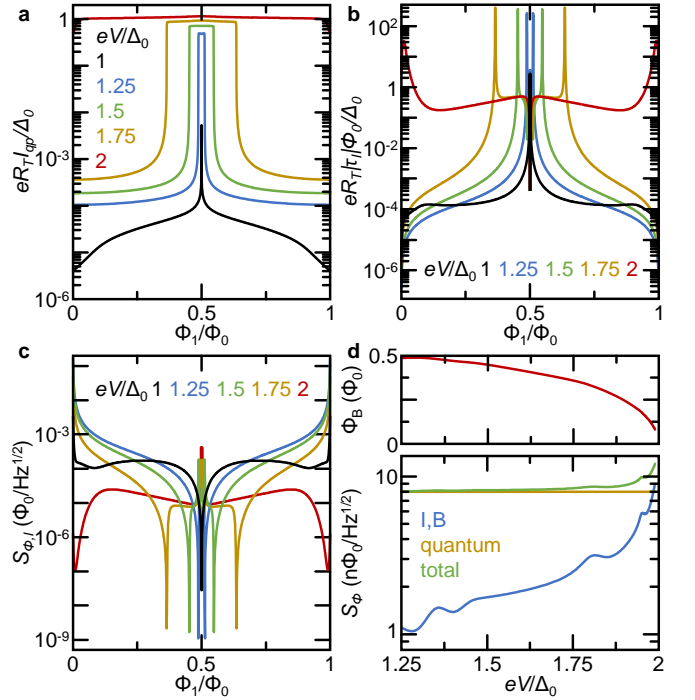

Figure 4. **Voltage bias operation.** (a) Quasiparticle current as a function of the external magnetic flux calculated for several values of V. (b) Flux-to-current transfer function versus Φ_1 calculated for different values of bias voltage. (c) Flux sensitivity per unit bandwidth as a function of Φ_1 for different values of V. In the calculations we set $R_T = 50$ kΩ and $\Delta_0 = 200$ μeV. (d) Top: Magnetic flux corresponding to best sensitivity versus V. Bottom: best flux sensitivity per unit bandwidth (blue) and quantum noise (gold) versus V. The total sensitivity is shown in green. All the panels assume $\beta = 0.8$, $\mathcal{L} = \mathcal{R} = 0.1$, $T = 0.01T_C$ and $\Gamma = 10^{-4}\Delta_0$.

2-b). As a consequence, the L-SQUIPT can be operated as a sensitive magnetometer by simple measurements of the output junction voltage in current bias mode or the tunneling quasiparticle current in voltage bias.

B. Voltage bias operation

The voltage bias operation of the L-SQUIPT magnetometer takes advantage of the strong Φ_1 dependence of I_{qp} for specific values of V, as shown in Fig. 4-a. In particular, the current is almost independent of the magnetic flux for $V = 2\Delta_0/e$, since the output junction is always biased in the normal-state. For lower values of the bias voltage, the modulation of E_g with Φ_1 results in the strong variation of I_{qp} with the magnetic flux. Indeed, by decreasing V the maximum steepness of the curves moves towards $\Phi_1 = 0.5\Phi_0$, that is reached for $V = \Delta_0/e$ thus corresponding to $E_g(\Phi_1) = 0$ (see Fig. 2-b). As a consequence, the voltage bias operation of the L-SQUIPT requires $\Delta_0 < eV < 2\Delta_0$.

The Φ_1 dependence of I_{qp} is completely reflected in the flux-to-current transfer function, which is defined as

$$\tau_I = \frac{dI_{qp}}{d\Phi_1}. \tag{16}$$

Figure 4-b shows τ_I versus Φ_1 calculated for the same parameters of I_{qp} (panel a). At a given V, the maximum value of the transfer function corresponds to the strongest variation of I_{qp} with Φ_1, while $\tau_I = 0$ for $\Phi_1 = 0.5\Phi_0$ (where I_{qp} shows its maximum, see Fig. 4-a).

The most common figure of merit for a magnetometer is the the flux noise, i.e., the flux sensitivity per unit bandwidth. In voltage bias operation, this can be written as

$$S_{\Phi,I} = \frac{\sqrt{S_I}}{|\tau_I|}, \tag{17}$$

where S_I is the current-noise spectral density. The latter reads

$$S_I = 2eI_{qp}(V)\coth\frac{eV}{2k_BT}. \tag{18}$$

Figure 4-c shows the Φ_1 dependence of $S_{\Phi,I}$ for the L-SQUIPT calculated at different values of bias voltage. For these simulations we assume a geometry and materials feasible by standard fabrication techniques. Indeed, we set $\Delta_0 = 200\ \mu$eV (aluminum) for the superconducting ring and the output tunnel probe while considering a tunnel resistance $R_T = 50$ kΩ. The flux sensitivity strongly depends on both Φ_1 and V. Indeed, depending on the magnetic flux of interest, the best operating point (Φ_B) can be chosen by tuning the bias voltage (see the top panel of Fig. 4-d). The flux noise corresponding to Φ_B is $S_{\Phi,I_{best}} < 10$ n$\Phi_0/\sqrt{\text{Hz}}$ for a bias voltage in the range $1.25\Delta_0 \leq eV < 2\Delta_0$. We note that, in a superconducting interferometer, the ultimate flux sensitivity is limited by the quantum noise ($S_{\Phi,q}$) defined as [28]

$$S_{\Phi,q} = \sqrt{\hbar L_1}. \tag{19}$$

By substituting $I_{C1} = 100\ \mu$A in the screening parameter equation, we obtain $L_1 = 2.6$ pH. The resulting quantum noise due to the inductance of the superconducting ring is $S_{\Phi,q} = 8$ n$\Phi_0/\sqrt{\text{Hz}}$. Therefore, the L-SQUIPT magnetometer operated in voltage bias shows a quantum limited flux sensitivity for most values of V. In fact, $S_{\Phi,q}$ dominates the total flux noise of the device, defined as $S_{\Phi,t} = \sqrt{s_{\Phi,I}^2 + S_{\Phi,q}^2}$, in almost the full voltage range (see bottom panel of Fig. 4-d).

C. Current bias operation

The current bias operation of the L-SQUIPT magnetometer exploits the dependence of V on Φ_1 while
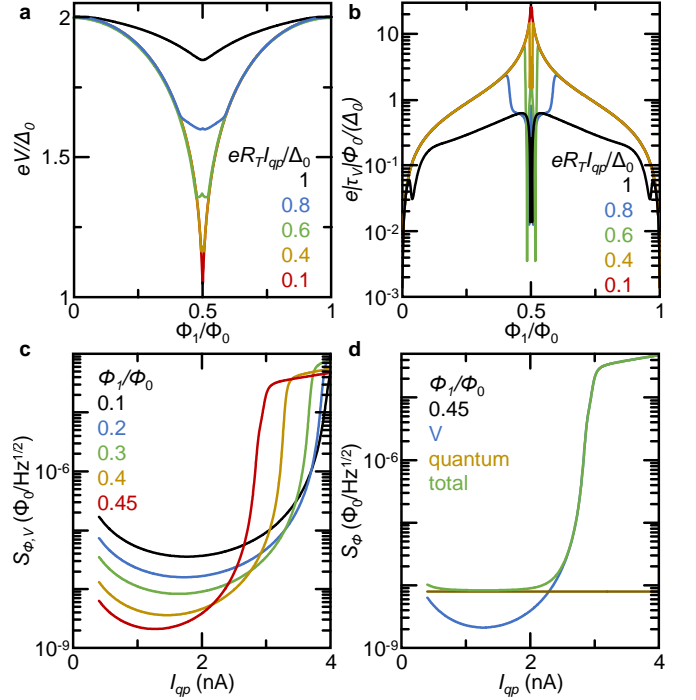

Figure 5. **Current bias operation.** (a) Output voltage as a function of the external magnetic flux calculated for several values of I_{qp}. (b) Flux-to-voltage transfer function versus Φ_1 calculated for different values of bias current. (c) Flux sensitivity per unit bandwidth as a function of I_{qp} for different values of Φ_1. In the calculations we employed $R_T = 50$ kΩ and $\Delta_0 = 200\ \mu$eV. (d) Flux sensitivity per unit bandwidth (blue) and quantum noise (gold) versus I_{qp} calculated for $\Phi_1 = 0.45\Phi_0$. The total sensitivity is shown in green. All the panels assume $\beta = 0.8$, $\mathcal{L} = \mathcal{R} = 0.1$, $T = 0.01T_C$ and $\Gamma = 10^{-4}\Delta_0$.

a constant I_{qp} is injected in the device, as shown in Fig. 5-a. For $I_{qp} = \Delta_0/(eR_T)$, the modulation of V with the external magnetic flux is limited, while by decreasing the bias current the voltage span and the steepness of the curves increase. This behavior is highlighted by the flux-to-voltage transfer function

$$\tau_V = \frac{dV}{d\Phi_1}. \tag{20}$$

Indeed, the maximum value of the transfer function rises while moving towards $0.5\Phi_0$ by increasing the bias current (see Fig. 5-b). In particular, the L-SQUIPT shows $\tau_V \simeq 26\Delta_0/(e\Phi_0)$ at $\Phi_1 = 0.498\Phi_0$ for $I_{qp} = 0.1\Delta_0/(eR_T)$.

In current bias operation, the flux sensitivity per unit bandwidth can be written as
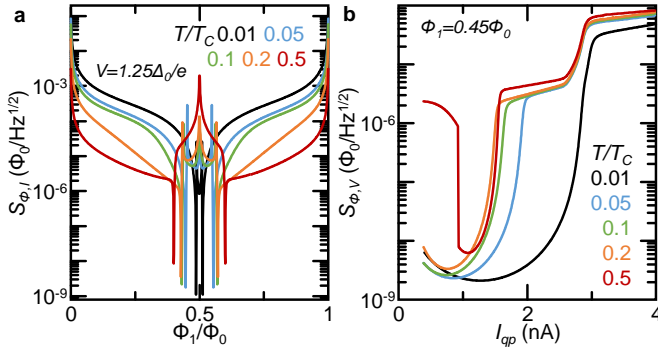
$$S_{\Phi,V} = \frac{\sqrt{S_V}}{|\tau_V|}, \tag{21}$$

Figure 6. **Temperature dependence of the flux sensitivity.** (a) Flux sensitivity per unit bandwidth as a function of Φ_1 for different values of temperature calculated at $V = 1.25\Delta_0/e$. (b) Flux sensitivity per unit bandwidth as a function of I_{qp} calculated for different values of temperature at $\Phi_1 = 0.45\Phi_0$. All the panels assume $\beta = 0.8$, $\mathcal{L} = \mathcal{R} = 0.1$, $\Gamma = 10^{-4}\Delta_0$, $R_T = 50$ kΩ and $\Delta_0 = 200$ μeV.

where the voltage-noise spectral density takes the form

$$S_V = R_d^2 S_I = \left(\frac{dV}{dI}\right)^2 S_I. \tag{22}$$

In the above equation, $R_d = dV/dI$ is the differential resistance of the output Josephson junction. Figure 5-c shows $S_{\Phi,V}$ as a function of I_{qp} for several values of Φ_1. For the simulations we considered the same structure of the voltage bias configuration, that is $\Delta_0 = 200$ μeV for both the superconducting ring and the output tunnel electrode ($R_T = 50$ kΩ). The L-SQUIPT sensitivity is maximum for high value of magnetic flux, as a result of the increased flux-to-voltage transfer function (see Fig. 5-b). In particular, a flux sensitivity of ~ 2 n$\Phi_0/\sqrt{\text{Hz}}$ can be reached for $\Phi = 0.45\Phi_0$ at $I_{qp} \simeq 1.3$ nA.

Also in the current bias mode, the L-SQUIPT magnetometer shows a quantum limited flux sensitivity. Indeed, $S_{\Phi,q} = 8$ n$\Phi_0/\sqrt{\text{Hz}}$ dominates the total flux noise of the device in a wide range of bias currents, as shown in Fig. 5-d for $\Phi = 0.45\Phi_0$.

D. Temperature dependence

Here, we investigate the temperature dependence of the L-SQUIPT performance both in voltage and in current bias. To this end, we set the same device parameters of previous sections, that is $\mathcal{L} = \mathcal{R} = 0.1$, $\Gamma = 10^{-4}\Delta_0$, $R_T = 50$ kΩ and $\Delta_0 = 200$ μeV. Since β is a temperature dependent parameter, we consider $\beta(T = 0.01T_C) = 0.8$ taking into account the exponential damping of I_{C1} with T [18]. Indeed, Eq 2 can be employed for $T \geq 0.05T_C$ in an aluminum/copper SNS junction of length $L = 2$ μm (with $D = 6 \times 10^{-3}$m^{2}s^{-1} the diffusion coefficient of copper).

Figure 6-a shows the flux sensitivity in the voltage bias operation (at $V = 1.25\Delta_0/e$) as a function of Φ_1 calculated for different values of T. By increasing the temperature, the best value of $S_{\Phi,I}$ rises substantially, while Φ_B is only slightly affected from T. On the contrary, the sensitivity far way from the best operating point improves by increasing temperature, since the flux-to-current transfer function shows a smoother dependence in Φ_1. Indeed, at high temperature, the CPR of J_2 shows a lower slope around $\varphi_2 = \pi$ (see Fig. 1-b), thus causing a smaller variation of I_{qp} with Φ_1. This degrades the best performance of the L-SQUIPT, but it provides a more constant sensitivity in the whole magnetic flux range (see the red curve in Fig. 6-a).

Figure 6-b shows the temperature dependence of the flux sensitivity of the L-SQUIPT operated in current bias at $\Phi_1 = 0.45\Phi_0$. By rising the temperature, the magnetometer best sensitivity is slightly affected by temperature, but the range fo bias current showing high sensitivity narrows. For $T = 0.5T_C$, a flux sensitivity $S_{\Phi,V} \sim 10$ n$\Phi_0/\sqrt{\text{Hz}}$ is obtained for $I_{qp} \sim 1$ nA. Thus, the L-SQUIPT is a quantum limited magnetometer both in voltage and current bias operations only for $T < 0.5T_C$.

V. DISSIPATIONLESS READ-OUT

Here, we discuss the magnetic flux dependent Josephson transport between J_2 and P. This will allow us to evaluate the sensitivity of the L-SQUIPT magnetometer in different dissipationless read-out geometries.

A. Josephson current and inductance

Since we assume a superconducting tunnel read-out probe, a dissipationless zero-bias current (I_{out}) can flow thanks to Josephson coupling. The latter can be calculated by means of the Ambegaokar-Baratoff equation for a point-like junction [17, 29]

$$I_{out}(T,\varphi_2) = \frac{\pi E_g(T,\varphi_2)\Delta(T)k_B T}{eR_T} \times$$
$$\sum_{l=0,\pm 1,\dots} \frac{1}{\sqrt{[\omega_l^2 + E_g^2(T,\varphi_2)][\omega_l^2 + \Delta^2(T)]}}, \tag{23}$$

where $\omega_l = \pi k_b T(2l + 1)$.

Figure 7-a shows I_{out} versus Φ_1 calculated for a L-SQUIPT at $T = 0.01$ T_C and $\mathcal{L} = \mathcal{R} = 0.1$ for different values of β. We consider the same structure of the previous calculations, that is $\Delta_0 = 200$ μeV and $R_T = 50$ kΩ. At $\Phi_1 = 0$, all the curves collapse to the same maximum value, that is the output junction critical current ($I_{C,out} \simeq 6.2$ nA). By rising the external magnetic flux, I_{out} lowers until reaching its minimum at

$\Phi_1 = 0.5\Phi_0$, because the superconducting energy gap of J_2 closes. The energy gap shows a steeper dependence on Φ_1 for large values of β (see Fig. 2-b). This behavior is transferred to the Josephson current. Indeed, the variation of I_{out} around $\Phi_1 = 0.5\Phi_0$ is less sharp for low values of the screening parameter (see Fig. 7-a).

The suppression of the critical current causes the variation of the Josephson inductance of the read-out junction ($L_{J_{out}}$). The latter can be calculated through Eq. 6 by considering the phase of the tunnel probe equal to 0. Consequently, $L_{J_{out}}$ is proportional to the derivative of φ_2 with respect to I_{out}. Figure 7-b shows $L_{J_{out}}$ versus Φ_1 calculated starting from the Josephson currents shown in panel a. For all values of β, the inductance spans over several orders of magnitude. By increasing β, the overall variation of $L_{J_{out}}$ with the magnetic flux increase and its maximum steepness moves from $\Phi_1 \to 0$ to $\Phi_1 \to 0.5\Phi_0$.

For the implementation of dissipationless read-out schemes, we need to consider the total inductance of the L-SQUIPT (L_{TOT}) represented in Fig. 7c. The small ring inductance L_2 and the second junction inductance L_{J_2} are in series. This block is in parallel with the inductance (L_{J_1}) of the junction J_1. The resulting inductance is in series with the large loop inductance L_1. All these are in series with the Josephson output tunnel junction inductance L_{out}. Thus, the total inductance is

$$L_{TOT}(\Phi_1) = L_1 + \frac{L_{J_1}(\Phi_1)[L_2 + L_{J_2}(\Phi_1)]}{L_2 + L_{J_1}(\Phi_1) + L_{J_2}(\Phi_1)} + L_{J_{out}}(\Phi_1). \tag{24}$$

The variation of Josephson inductance, and thus L_{TOT}, can be revealed through different dissipationless read-out schemes. Indeed, the L-SQUIPT can be inductively coupled to a SQUID amplifier, as routinely realized for kinetic inductance detectors (KIDs). Alternatively, the device can be integrated in a RLC resonant circuit, whose resonance frequency varies with Φ_1.

B. Inductive read-out

The scheme for the inductive read-out of the L-SQUIPT is shown in Fig. 8-a. The parallel connection of the L-SQUIPT (of inductance L_{TOT}) and a load inductor (L) is biased by means of a dc current current generator (I_b). Indeed, the variation of L_{TOT} generates a change of the current flowing through the L-SQUIPT (I_{out}) and the load resistor (I_L). The latter is detected by a dc SQUID inductively coupled to the circuit through the mutual inductance M, where the magnetic flux piercing the SQUID is $\Phi_s = MI_L$. For small variations of Φ_S (linear response regime, $LI_L \ll \Phi_0$) [30], the current flowing through the load inductor reads

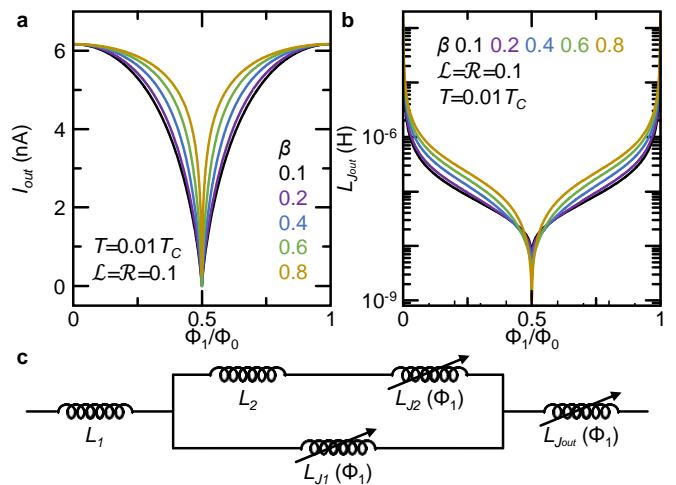$$I_L = I_b \frac{\Phi_0}{\Phi_0 + 2\pi L I_{out}}. \tag{25}$$

Figure 7. **Josephson transport through the read-out junction. (a)** Josephson current flowing through the output tunnel junction as a function of Φ_1 calculated for different values of β. **(b)** Kinetic inductance of the output tunnel junction as a function of Φ_1 calculated for different values of β. Both panels assume $\mathcal{L} = \mathcal{R} = 0.1$, $\Gamma = 10^{-4}\Delta_0$, $T = 0.01T_C$, $R_T = 50$ kΩ and $\Delta_0 = 200$ μeV. **(c)** Schematic representing all the components of the total inductance (L_{TOT}) of the L-SQUIPT. We represented all the inductance contributions that directly or indirectly depend on Φ_1.

In this configuration, the L-SQUIPT operates as a magnetic-flux-to-magnetic-flux transducer or magnetic flux amplifier, where the efficiency can be quantify by

$$\frac{d\Phi_S}{d\Phi_1} = \frac{dI_{out}}{d\Phi_1} M \frac{dI_L}{dI_{out}}. \tag{26}$$

The ratio $dI_{out}/d\Phi_1$ can be calculated through the derivative of Eq. 23 with respect of the input magnetic flux. Accordingly, the term dI_L/dI_{out} can be calculated by performing the dI_{out} derivative of Eq. 25, thus obtaining the following expression

$$\frac{dI_L}{dI_{out}} = 2\pi L I_b \frac{\Phi_0}{(\Phi_0 + 2\pi L I_{out})^2}. \tag{27}$$

C. Dispersive measurement

The scheme for the dispersive read-out of the L-SQUIPT is shown in Fig. 8-b, where the Φ_1-dependent variation of the Josephson inductance $L_{J_{out}}$ is determined by measuring the resonance frequency of a suited RLC circuit. To this end, a load inductance L_L is added in parallel to the total inductance of the L-SQUIPT (L_{TOT}). This circuit is coupled by a mutual inductance (M) with a tank circuit characterized by inductance L_T, capacitance C_T and resistance R_T. The resulting
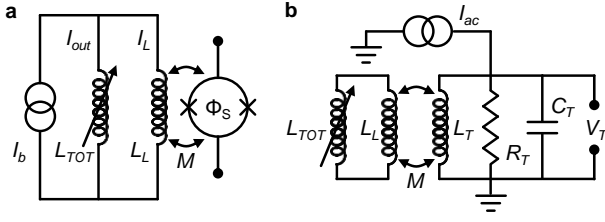
Figure 8. **Dissipationless read-outs for the L-SQUIPT.**
(a) Inductive read-out scheme, where the changes of the
L-SQUIPT inductance (L_{TOT}) are recorded by dc SQUID
magnetometer coupled to the device by a mutual inductance
M. **(b)** Dispersive read-out scheme, where the changes of
L_{TOT} are recorded thanks to the changes of the characteristic
frequency of a resonant circuit inductively coupled to the
L-SQUIPT.

effective inductance of the tank circuit is [31, 32]

$$\tilde{L}_T = L_T\Big(1 - \frac{M^2}{L_T}\frac{1}{L_{TOT}(\Phi_1)+L_L}\Big). \quad (28)$$

As a consequence, the resonance frequency of the tank
circuit $\tilde{f}_T = 1/2\pi\sqrt{\tilde{L}_T C_T}$ strongly depends on the flux
Φ_1.

D. L-SQUIPT noise in dissipationless read-out operation

We assume that the read-out circuit in Fig. 8
has negligible noise so that the overall sensitivity of
L-SQUIPTis determined by its intrinsic noise associated
to each element of the device and their correlations.

From Fig. 8 we can see that noise is essentially
determined by the fluctuations of the current across the
load inductance L_L that is then coupled my mutual
inductance with the read-out circuit. The current of
interest is the tunnel junction one I_{out} in Eq. 23. This
is composed by a Johnson thermal contribution (related
to the resistances of Josephson junctions) and a phase
contribution.

The first one is dominated by the tunnel resistance R_T
that is much larger than R_{J_1} and R_{J_2}. For a frequency
bandwidth $\delta\omega/(2\pi)$, it generates a noise voltage of means
square value [31]

$$\langle\delta V^2_{J_{out}}\rangle = 4k_BTR_T\frac{\delta\omega}{2\pi}. \quad (29)$$

The tunnel junction can be e represented by an
RLC parallel circuit with resistance R_T, a Josephson
inductance $L_{J_{out}}$ and a small capacitance C_{out}. Passing
to the frequency dependent impedances, i.e., $Z_{R_T} = R_T$,
$Z_{L_{J_{out}}} = i\omega L_{J_{out}}$, and $Z_{C_{J_{out}}} = 1/(i\omega C_{out})$, for the
junction J_{out} we have an impedance

$$\frac{1}{Z_{J_{out}}} = \frac{1}{Z_{R_T}} + \frac{1}{Z_{L_{J_{out}}}} + \frac{1}{Z_{C_{J_{out}}}}. \quad (30)$$

As a consequence, the mean square of the current noise
due to the resistance can be written [31, 33]

$$\langle\delta I^2_{out,R}\rangle = \frac{\langle\delta V^2_{J_{out}}\rangle}{|Z_{J_{out}}|^2} = \frac{4k_BTR_T}{|Z_{J_{out}}|^2}\frac{\delta\omega}{2\pi}. \quad (31)$$

The phase noise contribution to I_{out} is due to the fact
that, as seen in Eq. 23, I_{out} depends on the phase φ_2. To
calculate it, we first consider the Johnson noise generated
by the two separate junctions J_1 and J_2 at temperature
T. Analogously, to what done for the tunnel junction,
we have that the noise is

$$\langle\delta I^2_{J_i}\rangle = \frac{\langle\delta V^2_{J_i}\rangle}{|Z_{J_i}|^2} = \frac{4k_BTR_{J_i}}{|Z_{J_i}|^2}\frac{\delta\omega}{2\pi}. \quad (32)$$

with $i = 1,2$ and Z_{J_i} is obtained by Eq. 30 with the
index exchanges.

These uncorrelated noise sources are conbined in the
following way. The small loop can be treated as a SQUID
with two Josephson junctions in parallel. Following Ref.
[31], we consider the circulating current I_{circ} as a function
of the current flowing through the junction J_1 and J_2:
$I_{circ} = I_{J_1} - I_{J_2}$.

The fluctuations of the circular current coupled with
the loop impedance L_2 and determines the phase
fluctuations $\delta\varphi_2$. They can be written as $\langle\delta I^2_{circ}\rangle = \langle\delta I^2_{J_1}\rangle + \langle\delta I^2_{J_2}\rangle$. By multiplying this expression by
$4\pi^2L_2^2/\Phi_0^2$ and using Eq. 32, we obtain the mean square
of the phase noise

$$\langle\delta\varphi^2_2\rangle = \frac{16\pi^2k_BTL_2^2}{\Phi_0^2}\Big(\frac{R_{J_1}}{|Z_{J_1}|^2} + \frac{R_{J_2}}{|Z_{J_2}|^2}\Big)\frac{\delta\omega}{2\pi}. \quad (33)$$

The noise current of the tunnel junction is sum of the
square of the thermal and phase noise (Eqs. 31 and 33,
respectively)

$$\langle\delta I^2_{out}\rangle = \frac{4k_BTR_T}{|Z_{J_{out}}|^2}\frac{\delta\omega}{2\pi} + c_{\varphi_2}\langle\delta\varphi^2_2\rangle. \quad (34)$$

The coefficient c_{φ_2} is obtained from Eqs. 13 and 23 taking
a small variation of I_{out} a a function of φ_2

$$c_{\varphi_2} = \frac{1}{4}\Big(\frac{\pi\Delta^2(T)k_BT}{eR_T}\Big)^2\sin^2\frac{\varphi_2}{2}$$
$$\Big[\sum_l\frac{1}{\sqrt{[\omega_l^2 + E_g^2(T,\varphi_2)][\omega_l^2 + \Delta^2(T)]}}\Big]^2. \quad (35)$$

Finally, the current fluctuations across L_L induce flux
fluctuations

$$\langle\delta\Phi^2_L\rangle = \langle\delta I^2_{out}\rangle L_L^2. \quad (36)$$

This is the intrinsic magnetic flux noise of the L-SQUIPT
that is the ultimate limit the sensitivity of the
measurement through the read-out circuit in Fig. 8.

We note that the performance for the dissipationless
read-out of a L-SQUIPT depend non-trivially on R_T, $\delta\omega$

and Φ_1. On the one hand, increase of R_T and $\delta\omega$ increase both contributions of $\langle\delta I_{out}^2\rangle$ (see Eq. 34). On the other hand, large values of R_T and $\delta\omega$ increase $Z_{J_{out}}$ (see Eq. 30) thus suppressing the current noise. Similarly, Φ_1 acts on several quantities in Eq. 34 with unexpected consequences. In particular, the noise is minimum for $\Phi_1 \to 0$ ($\varphi_2 \to 0$), since phase noise contribution becomes negligibly small, as shown by Eq. 35. The best magnetic flux fluctuation for a L-SQUIPT operated in dissipationless mode is $\langle\delta\Phi_L\rangle \sim 4\ \mu\Phi_0$ obtained at $\Phi_1 = 0$ for $\mathcal{L} = \mathcal{R} = 0.1$, $\Gamma = 10^{-4}\Delta_0$, $T = 20$ mK, $R_T = 50$ kΩ, $\Delta_0 = 200\ \mu$eV, $\delta\omega/2\pi = 100$ MHz, $C_{J_{out}} = 1$ fF and $L_L = 10$ pH.

VI. CONCLUSIONS

In conclusion, we have proposed and theoretically investigated an innovative highly sensitive magnetometer: the inductive superconducting quantum interference proximity transistor (L-SQUIPT). The L-SQUIPT promises enhanced performance with respect to widespread SQUID and SQUIPT magnetometers. Indeed, an L-SQUIPTs made of conventional materials (such as aluminum and copper) would show a quantum limited intrinsic noise down to ~ 8 n$\Phi_0/\sqrt{\text{Hz}}$, both in current and voltage bias operations. Furthermore, the superconducting output probe allows to design two different dissipationless read-out schemes based on the variation of the Josephson inductance of the tunnel junction, such as inductive and dispersive read-out setups. In these configurations, the best flux fluctuation is $\langle\delta\Phi_L\rangle \sim 4\ \mu\Phi_0$ for a bandwidth of 100 MHz.

[1] R. Cantor and D. Koelle, *Practical DC SQUIDS: Configuration and Performance* (John Wiley & Sons, Ltd, 2004), chap. 5, pp. 171–217, ISBN 9783527603640.

[2] R. C. Jaklevic, J. Lambe, A. H. Silver, and J. E. Mercereau, Phys. Rev. Lett. **12**, 159 (1964), URL https://link.aps.org/doi/10.1103/PhysRevLett.12.159.

[3] D. Vasyukov, Y. Anahory, L. Embon, D. Halbertal, J. Cuppens, L. Neeman, A. Finkler, Y. Segev, Y. Myasoedov, M. L. Rappaport, et al., Nature Nanotech **8**, 639 (2013), URL https://link.aps.org/doi/10.1103/PhysRevB.85.024527.

[4] F. Giazotto, J. T. Peltonen, M. Meschke, and J. P. Pekola, Nature Physics **6**, 254 (2010), URL https://www.nature.com/articles/nphys1537.

[5] M. Meschke, J. T. Peltonen, J. P. Pekola, and F. Giazotto, Phys. Rev. B **84**, 214514 (2011), URL https://link.aps.org/doi/10.1103/PhysRevB.84.214514.

[6] A. Ronzani, C. Altimiras, and F. Giazotto, Phys. Rev. Applied **2**, 024005 (2014), URL https://link.aps.org/doi/10.1103/PhysRevApplied.2.024005.

[7] R. N. Jabdaraghi, M. Meschke, and J. P. Pekola, Applied Physics Letters **104**, 082601 (2014), https://doi.org/10.1063/1.4866584, URL https://doi.org/10.1063/1.4866584.

[8] S. D'Ambrosio, M. Meissner, C. Blanc, A. Ronzani, and F. Giazotto, Applied Physics Letters **107**, 113110 (2015), https://doi.org/10.1063/1.4930934, URL https://doi.org/10.1063/1.4930934.

[9] R. N. Jabdaraghi, J. T. Peltonen, O.-P. Saira, and J. P. Pekola, Applied Physics Letters **108**, 042604 (2016), https://doi.org/10.1063/1.4940979, URL https://doi.org/10.1063/1.4940979.

[10] R. N. Jabdaraghi, D. S. Golubev, J. P. Pekola, and J. T. Peltonen, Scientific Reports **7**, 8011 (2017), https://doi.org/10.1038/s41598-017-08710-7, URL https://doi.org/10.1038/s41598-017-08710-7.

[11] P. Virtanen, A. Ronzani, and F. Giazotto, Phys. Rev. Applied **6**, 054002 (2016), URL https://link.aps.org/doi/10.1103/PhysRevApplied.6.054002.

[12] A. Ronzani, S. D'Ambrosio, P. Virtanen, F. Giazotto, and C. Altimiras, Phys. Rev. B **96**, 214517 (2017), URL https://link.aps.org/doi/10.1103/PhysRevB.96.214517.

[13] N. Ligato, G. Marchegiani, P. Virtanen, E. Strambini, and F. Giazotto, Scientific Reports **7**, 8810 (2016), URL https://www.nature.com/articles/s41598-017-09036-0.

[14] P. G. De Gennes, *Superconductivity of Metals and Alloys*, Advanced book classics (Perseus, Cambridge, MA, 1999), URL https://cds.cern.ch/record/566105.

[15] A. I. Buzdin, Rev. Mod. Phys. **77**, 935 (2005), URL https://link.aps.org/doi/10.1103/RevModPhys.77.935.

[16] F. Zhou, P. Charlat, B. Spivak, and B. Pannetier, Journal of Low Temperature Physics **110**, 841 (1998), URL https://doi.org/10.1023/A:1022628927203.

[17] F. Giazotto and F. Taddei, Phys. Rev. B **84**, 214502 (2011), URL https://link.aps.org/doi/10.1103/PhysRevB.84.214502.

[18] A. A. Golubov, M. Y. Kupriyanov, and E. Il'ichev, Rev. Mod. Phys. **76**, 411 (2004), URL https://link.aps.org/doi/10.1103/RevModPhys.76.411.

[19] K. K. Likharev, Rev. Mod. Phys. **51**, 101 (1979), URL https://doi.org/10.1103/RevModPhys.51.101.

[20] H. le Sueur, P. Joyez, H. Pothier, C. Urbina, and D. Esteve, Phys. Rev. Lett. **100**, 197002 (2008), URL https://link.aps.org/doi/10.1103/PhysRevLett.100.197002.

[21] T. T. Heikkilä, J. Särkkä, and F. K. Wilhelm, Phys. Rev. B **66**, 184513 (2002), URL https://link.aps.org/doi/10.1103/PhysRevB.66.184513.

[22] N. Ligato, E. Strambini, F. Paolucci, and F. Giazotto, Nature Communications **12**, 5200 (2021), URL https://doi.org/10.1038/s41467-021-25209-y.

[23] M. Polini, F. Giazotto, K. C. Fong, I. M. Pop, C. Schuck, T. Boccali, G. Signorelli, M. D'Elia, R. H. Hadfield, V. Giovannetti, et al., arXiv preprint arXiv:2201.09260 (2022).

[24] I. O. Kulik and A. N. Omel'yanchuk, JEPT Lett. **21**, 96 (1975).

[25] S. N. Artemenko, A. F. Volkov, and A. V. Zaitsev, Sov. Phys. JEPT **49**, 924 (1979).

[26] R. C. Dynes, J. P. Garno, G. B. Hertel, and T. P. Orlando, Phys. Rev. Lett. **53**, 2437 (1984), URL https://link.aps.org/doi/10.1103/PhysRevLett.53.2437.

[27] M. Tinkham, *Introduction to superconductivity* (Courier Dover Publications, 2012).

[28] J. R. Kirtley, Reports on Progress in Physics **73**, 126501 (2010), URL https://doi.org/10.1088/0034-4885/73/12/126501.

[29] V. Ambegaokar and A. Baratoff, Phys. Rev. Lett. **10**, 486 (1963), URL https://link.aps.org/doi/10.1103/PhysRevLett.10.486.

[30] F. Giazotto, T. T. Heikkilä, G. P. Pepe, P. Helistö, A. Luukanen, and J. P. Pekola, Applied Physics Letters **92**, 162507 (2008), https://doi.org/10.1063/1.2908922, URL https://doi.org/10.1063/1.2908922.

[31] A. Barone and G. Paterno, *Physics and applications of Josephson effect* (Wiley New York, 1982), ISBN 0471014699,9780471014690.

[32] C. Guarcello, P. Solinas, A. Braggio, M. Di Ventra, and F. Giazotto, Phys. Rev. Applied **9**, 014021 (2018), URL https://link.aps.org/doi/10.1103/PhysRevApplied.9.014021.

[33] P. Solinas, M. Möttönen, J. Salmilehto, and J. P. Pekola, Phys. Rev. B **85**, 024527 (2012), URL https://link.aps.org/doi/10.1103/PhysRevB.85.024527.